Hindawi
Mathematical Problems in Engineering
Volume 2020, Article ID 1424167, 11 pages
https://doi.org/10.1155/2020/1424167

Research Article

Shear Effects on the Anchorage Interfaces and Seismic Responses of a Rock Slope Containing a Weak Layer under Seismic Action

Zhe Long[1], **Zhi-xin Yan**[1,2] **and Chun-bo Liu**[2]

[1]*School of Civil Engineering and Mechanics, Lanzhou University, Lanzhou 730000, China*
[2]*School of Civil and Transportation Engineering, Henan University of Urban Construction, Pingdingshan 467036, China*

Correspondence should be addressed to Zhi-xin Yan; yzx10@163.com

Received 25 November 2019; Accepted 15 February 2020; Published 30 April 2020

Academic Editor: Francesco Tornabene

The shear effects on the anchorage interfaces under seismic action is a key problem requiring urgent investigation in the field of rock and soil anchorages. In this paper, the model of rock slope with a weak layer was constructed by pouring, and the large-scale shaking table model test was completed. The shear strain on the anchorage interfaces and the acceleration of the slope were collected using built measurement systems. The shear effects on the two anchorage interfaces (a bolt-grout interface and a grout-rock interface) and seismic responses of the slope under seismic action were investigated. The distribution laws of the shear stress on the two anchorage interfaces along the axial direction of the bolt under seismic action were gained. The variations of the peak acceleration amplification coefficient on the slope surface, the magnitude, and the growth rate of peak shear stress on the anchorage interfaces under seismic action with different excitation directions and intensities were obtained. Furthermore, the positive relationship between the shear effect on the anchorage interfaces and the seismic response of slope was revealed. This study provides support for theoretical research, numerical simulation analysis, and aseismic design of rock and soil anchorages under dynamic conditions.

1. Introduction

Anchoring, as a common method for supporting rock and soil masses, is extensively used in projects and plays a critical role in major projects due to its unique advantages such as delicate structures, ease of construction, low cost, and high performance; however, research into mechanisms used for anchoring slopes under seismic action lags far behind engineering practice, so it is necessary to study the shear effects on anchorage interfaces and the transfer of force in slopes under seismic action.

Numerous researchers have conducted in-depth studies on the action of force on anchorage interfaces under static action [1–7], and some have studied the seismic response of anchored slopes by conducting shaking table tests; however, there are seldom investigations made of the mechanism of anchoring rock and soil mass under dynamic action, which has restricted the application of anchoring technologies of rock and soil mass and the progress of relevant research thereinto [8–11]. Hong et al. [12] studied the seismic response of slopes anchored with soil nails under seismic action. Jian-Bin et al. [13] investigated the seismic response of lattice beams in slopes supported with framed anchor bolts. Qiu-Xiang et al. [14] explored the changing characteristics of loads on supports and displacement of slopes of Zipingpu reservoir before and after the Wenchuan earthquake (Wenchuan, Sichuan Province, China on 12 May 2008). Zhi-Xin et al. [15] investigated the dynamic response of a rock slope covered with red clay supported with anchor bolts and the distribution of axial forces on anchor bolts under seismic action.

Therefore, the authors first studied the shear effects on the bolt-grout interface and the grout-rock interface in a rock slope containing a weak layer and the seismic response

of the slope under seismic action by conducting large-scale shaking table model tests. In this way, the research of our team attempts to provide guidance to engineers interested in similar theoretical research, numerical simulation and analysis, and aseismic design.

2. Design of the Shaking Table Model Test

2.1. Similarity Ratio and Parameters of Similar Materials. The shaking table model tests need to obey three main theorems of similarity theory, by which the similarity ratio of the test model was determined. By considering the ratios of similar materials and preparation of the model, the geometric similarity ratio of the slope model to the prototype was determined as 1 : 8. The similarity ratios of various physical quantities are listed in Table 1.

The test model was constructed using the casting method, so the similar materials also should have a certain fluidity and a reasonable consolidation time when their physicomechanical parameters satisfied the similarity ratios. Through numerous experiments on ratios of the similar materials, finally barite, iron powder, and quartz sand were used as aggregates while gypsum and cement were used as cementitious materials. Other auxiliary materials included calcium carbonate, talc powder, glycerol, and water reducer. In this way, similar materials for constructing bedrock, unstable rock, a weak layer, and the grout in the test model of the slope were prepared, and the ratios of similar materials used for constructing bedrock, unstable rock, grout, and the weak layer could be attained (Tables 2 and 3). Moreover, by conducting a tensile test, aluminium tubes with outer and inner diameters of 5 mm and 4 mm, separately, were selected as the similar material to represent the bolt. The physicomechanical parameters of the similar materials in each part of the test model are listed in Table 4.

2.2. Model Size and Layout of Monitoring Points. The interior of the model box measured 3.0 m × 1.2 m × 2.0 m. On the bottom plate of the model box, a layer of sandy gravel, 20 mm thick, was placed, to avoid relative displacement between the bottom of the test model of the slope and the bottom plate of the box during seismic loading. Vaseline® was smeared on Perspex® sheets on two sides of the model box parallel to the direction of seismic excitation to reduce the frictional resistance between the box walls and the model. A wave-absorbing layer composed of a polystyrene foam board (80 mm thick) and a sheet of rubber latex foam (20 mm thick) was pasted on the front and back walls of the box, respectively, to enhance the wave-absorbing ability of the boundaries and reduce the constraints of the box walls on the deformation of the model. The cast model of the slope is illustrated in Figure 1.

The geometric dimensions of the cast model of the slope are shown in Figure 2. The model was 2.8 m long and 1.83 m high and consisted of two parts: the slope and the base. The slope in the upper part had a height of 1.5 m and a slope angle of 75°. The weak layer in the slope was 20 mm thick and made an included angle of 54° with the horizontal plane. The base below the slope measured 2.8 m × 1.2 m × 0.33 m.

Table 1: Similarity ratios in the shaking table model tests.

Frequency f	0.35
Elastic modulus E	8
Vibration time t	2.83
Stress σ	8
Cohesion c	8
Internal friction angle φ	1
Strain ε	1
Force F	512
Shear stress τ	8

Nine anchor bolts were arranged in a three-by-three rectangular array, with a horizontal spacing of 0.3 m and a vertical spacing of 0.375 m. The anchor bolts, with a rod diameter of 5 mm and a grout layer of 5 mm thick, were set so as to make an included angle of 15° with the horizontal plane. Strain gauges were pasted only on the three anchor bolts in the middle line, which served to monitor strains in the bolt-grout interface and the grout-rock interface.

2.3. Layout of Acceleration and Strain Monitoring Points. To monitor the acceleration seismic response of slope, acceleration sensors were set in the slope and on the slope surface, as shown in Figure 2. It can be seen from the figure that monitoring points for acceleration with a vertical spacing of 300 mm on the slope surface were A8 to A13, among which A13 was arranged in the bedrocks at the foot of the slope. Monitoring points for acceleration in the slope included A1 to A7. Two unidirectional acceleration sensors were arranged at each monitoring point, to collect accelerations in the X and Z-directions at the corresponding position, separately.

Among the three monitored anchor bolts, the upper one was anchored in the vicinity of the slope shoulder, where the seismic response was the most intense, so the anchoring effect was the most prominent. Therefore, the upper anchor bolt was selected as the main research object. The layout of strain gauges on the upper anchor bolt is illustrated in Figure 3. The strain gauges on the bolt-grout interfaces were numbered 1 to 10, and those at corresponding positions on the grout-rock interface were labelled A to J. The number increased from head to root of the anchor bolts along the axis thereof, that is, increased from unstable rocks to the interior of bedrocks. According to a literature review and previous research [16–18], the sections of the anchor bolts corresponding to the weak layer were taken as the key monitoring sections for strain in the two anchorage interfaces, where strain gauges were more closely spaced. Besides, two strain gauges were separately pasted on the bolt-grout interface and the grout-rock interface symmetrically about the same position of the anchor bolt in the key monitoring sections, in which one at each position was spare.

2.4. Loading Scheme in the Test. Wolong waves recorded in the Wenchuan earthquake in 2008 were used as input seismic waves, as shown in Figure 4. Acceleration amplitudes (intensity of

Table 2: Ratios (mass ratios) of materials for constructing rock mass and grout.

Materials	Barite	Iron powder	Quartz sand	Gypsum	Cement	Glycerol	Water	Retarder	Water reducer
Bedrock	180	120	150	105	45	12	65	6	0
Unstable rock	200	132	168	55	45	12	52	0	3
Grout	324	0	216	20	40	12	56	0	2.5

Table 3: Ratios (mass ratios) of materials for constructing the weak layer.

Materials	Barite	Iron powder	Talc powder	Calcium carbonate	Gypsum	Glycerol	Water	Water reducer
Weak layer	120	240	100	120	30	18	103	6

Table 4: Physicomechanical parameters of materials used to establish the model.

Sections	Density ($g \cdot cm^{-3}$)	Elastic modulus (GPa)	Compressive strength (MPa)	Tensile strength (MPa)	Cohesion (MPa)	Internal friction angle (°)
Bedrock	2.41	1.10	10.90	0.74	3.10	31.0
Unstable rock	2.52	0.91	5.20	0.44	1.70	27.2
Weak layer	1.93	0.01	0.16	—	0.06	24.0
Grout	2.58	0.47	3.44	0.20	0.34	39.5
Bolt	0.97	23.06	—	93.1	—	—

Figure 1: Model of the slope.

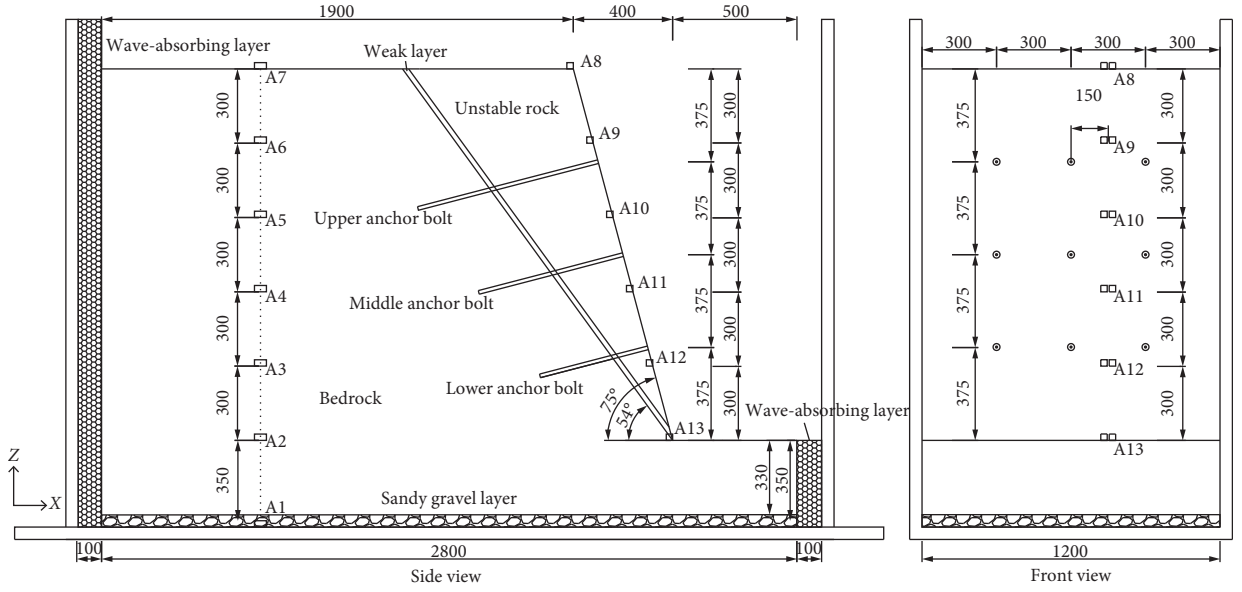

Figure 2: Model size and layout of monitoring points (unit: mm).

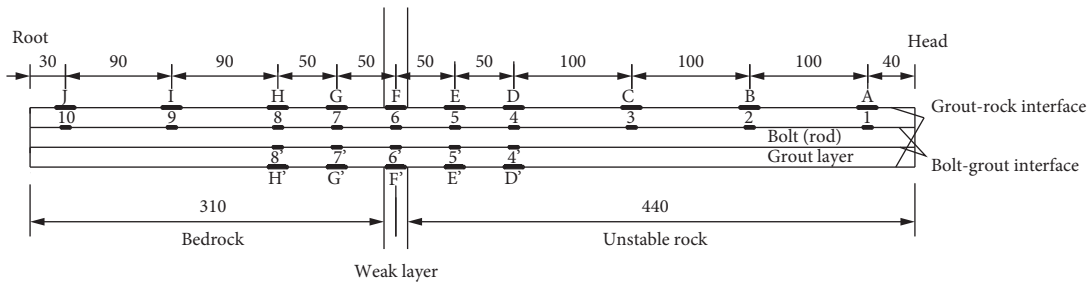

Figure 3: Top view of positions of strain gauges on the upper anchor bolt (unit: mm).

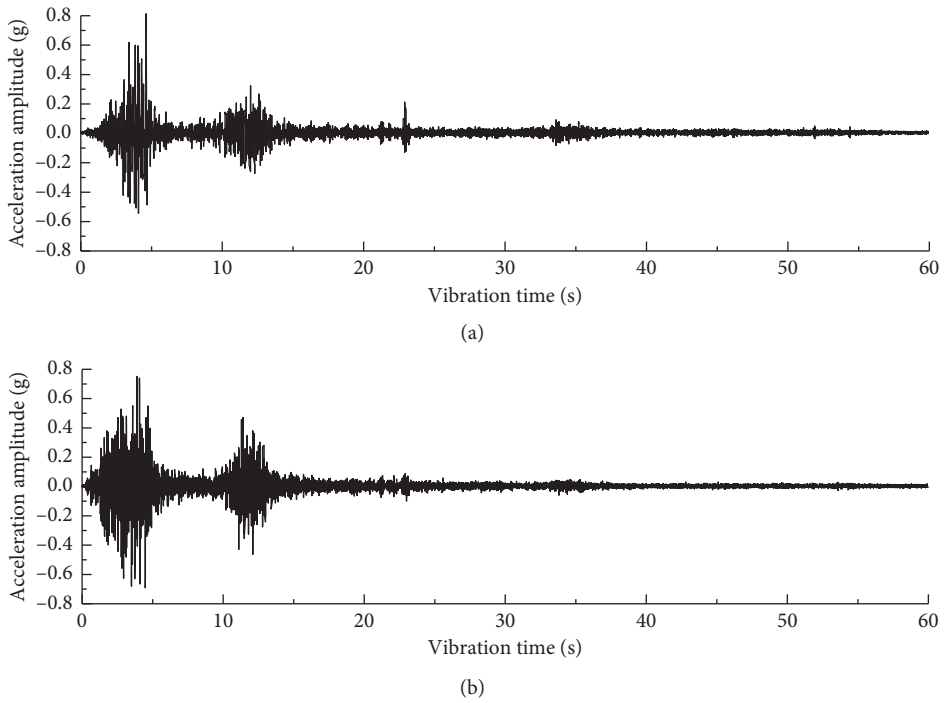

Figure 4: Wolong waves input by the shaking table. (a) Excitation in the X-direction. (b) Excitation in the Z-direction.

ground motion) and excitation directions (Z-unidirection, X-unidirection, and X and Z bidirection) of the seismic waves were changed after conducting similarity relationship convection, filtering, and baseline correction on the Wolong waves, which were then applied using the shaking table. During loading, the acceleration amplitude of seismic waves was taken as the main controlled variable, which was 0.1 g at the initial moment of loading and increased by in increments of 0.1 g. At each amplitude, seismic waves were excited in Z-unidirection, X-unidirection, and both the X and Z bidirections (seismic waves input in X and Z directions together). When applying seismic waves in the X and Z bidirection, the amplitude of X-direction seismic waves therein was identical to those applied in the X-unidirection: the amplitude of Z-direction seismic waves was 65% of that applied in the X-direction, which conformed to codified requirements for aseismic design [19].

3. Discussion of the Shaking Table Test Results

In the test, the strain gauge (F, around the upper anchor bolt) on the grout-rock interface of the upper anchor bolt in the weak layer took the lead in recording strain when acceleration amplitudes of Wolong waves input in X-unidirection and X and Z bidirection were increased to 0.4 g and those in the Z-unidirection augmented to 0.5 g, while at the same time, no response was monitored at strain gauges on the bolt-grout interface. On this basis, it was inferred that the top of the slope was the position where tensile deformation appeared first under the action of seismic waves. Therefore, to restrain the slope deformation, the anchor system began to take effect and the grout-rock interface of the upper anchor bolt was the first to experience a shear effect.

3.1. Acceleration Response. The seismic response of a slope is closely related to working mechanism of an anchor system, and analysing the seismic response of the slope thereby is helpful for ascertaining the shear effects on the anchorage interfaces. Therefore, the most representative seismic response, acceleration response of the slope surface, was selected for analysis.

The ratio coefficient of peak acceleration at any monitoring points ($A8$ to $A12$) on the slope surface to peak

acceleration in the same direction at monitoring point $A13$ at slope foot was defined as the peak acceleration amplification coefficient on slope surface. The foot of the slope (point $A13$) was defined as the datum for the elevation for the slope surface, and the elevation was positively vertically upward.

Figures 5 and 6 show the relationships of the peak acceleration amplification coefficients of the slope surface under effects of Wolong waves of different acceleration amplitudes and excitation directions with the elevation of the slope surface. As shown in Figure 5(a), when seismic waves were excited in the X-unidirection, peak acceleration amplification coefficients in the X-direction of slope surface for seismic response of the slope approximately linearly increased with the elevation of monitoring points and reached a peak at monitoring point $A8$ at the slope shoulder. As the acceleration amplitude of input motions was increased from 0.5 g to 0.8 g, the peak acceleration amplification coefficients in the X-direction at various monitoring points on the slope surface increased, and the upper part of the slope (90 to 150 cm) where the upper anchor bolt was arranged exhibited an increasingly prominent elevation amplification effect.

As shown in Figure 5(b), the peak acceleration amplification coefficients in the Z-direction at various monitoring points on the slope surface presented an increasing trend with the elevation of the monitoring points when the acceleration amplitude of the input motions in Z-unidirection was between 0.5 g and 0.7 g, while the peak acceleration amplification coefficient in the upper part of the slope surface (point $A9$) remained constant and in some cases decreased. At the same monitoring point on the slope surface, the peak acceleration amplification coefficient in the Z-direction grew rapidly with the increased acceleration amplitude of the Wolong waves. As the acceleration amplitude was increased to 0.8 g, peak acceleration amplification coefficients at various points all increased, showing prominent elevation amplification effects along the slope surface in an upward direction; however, the rate of growth of the peak acceleration amplification coefficient decreased with increasing elevation.

It can be seen from Figure 6 that the elevation amplification effect on the acceleration in X and Z directions was inconspicuous in the lower part of the slope while it was more apparent in the upper part if the Wolong waves with acceleration amplitudes of 0.5 g and 0.6 g were excited in the X and Z bidirection. When the acceleration amplitudes of Wolong waves were 0.7 g and 0.8 g, the changes in the peak acceleration amplification coefficients in the X and Z directions were similar to those when Wolong waves were separately input in the X-unidirection and Z-unidirection. By comparing Figures 5(a) and 6(a), the maximum value of peak acceleration amplification coefficient in the X-direction under excitation along the X-unidirection was larger than the corresponding value under excitation along the X and Z bidirection. This indicated that when Wolong waves were excited in the X and Z bidirections, the resultant vibration in the two directions generated a lower PGA amplification coefficient in the X-direction, rather than enhancing the acceleration seismic response.

The above analysis revealed that peak acceleration amplification coefficients in the X and Z directions at various monitoring points on the slope surface increased with the acceleration amplitude of the input seismic waves when unidirectional or bidirectional synthesised seismic waves were excited. Peak acceleration amplification coefficients in the X-direction on the slope surface all increased in a quasilinear manner with increasing elevation, while this increasing trend slowed down in the Z-direction. As the acceleration amplitude of input seismic waves was augmented, the surface of the upper part of the slope exhibited increasingly significant elevation amplification effects.

3.2. Response at Strain Monitoring Points. The strain and axial force of anchor bolts and shear stress on the two anchorage interfaces presented similar trends under various conditions when the model was in the elastic deformation stage. Considering this, the condition of input motion at 0.8 g in the X-unidirection was taken as an example for analysis. Figure 7 shows the time-history curves of strain recorded at point 6 on the bolt-grout interface and at point F on the grout-rock interface of the upper anchor bolt at the weak layer. In the figure, positive (negative) strain showed that the anchor bolt was in tension (in compression). The comparison of Figures 7(a) and 7(b) suggested that the two curves were consistent, i.e., the peak tensile strain and peak compressive strain appeared at 4.09 s and 4.62 s, respectively, on both curves, which coincided with the occurrence of positive and negative peaks on the time-history curves of seismic wave velocity in Figure 8. The result indicates that the shear effects on the anchorage interfaces were closely associated with the seismic response of the slope.

A slope lies in the most dangerous state when unstable rocks therein have the largest tendency to move to the free face relative to bedrock. Under that condition, the corresponding tensile strain and axial force are a peak strain and peak axial force, respectively. As shown in Figure 7, monitoring point 6 on the bolt-grout interface recorded the peak strain (5.31×10^{-5}) at 4.09 s under loading with Wolong waves at 0.8 g in the X-unidirection; at the same moment, the peak strain (1.45×10^{-4}) was recorded at monitoring point F on the grout-rock interface, with the former being only 36.6% of the latter. It indicated that seismic response on the grout-rock interface was greater than that of the bolt-grout interface.

Axial forces at various monitoring points can be calculated according to strain at 4.09 s, and then average shear stress on the section of the anchor bolt between two adjacent monitoring points can be computed based on the axial forces at the two points. The specific calculation process is as follows:

(1) Axial force F_i at the ith monitoring point can be calculated using formula (1) based on Hooke's law when the anchor bolt or the grout layer is deformed:

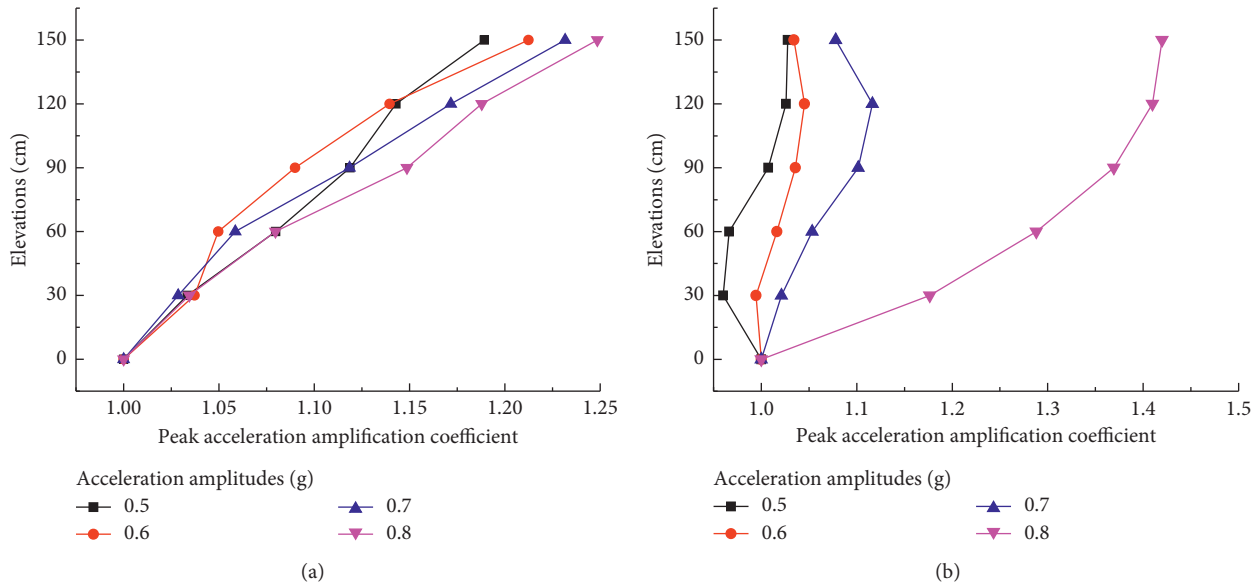

Figure 5: Changes in peak acceleration amplification coefficients of the slope surface with elevation under excitation in the unidirection. (a) Acceleration in the X-direction under excitation in the X-unidirection. (b) Acceleration in the Z-direction under excitation in the Z-unidirection.

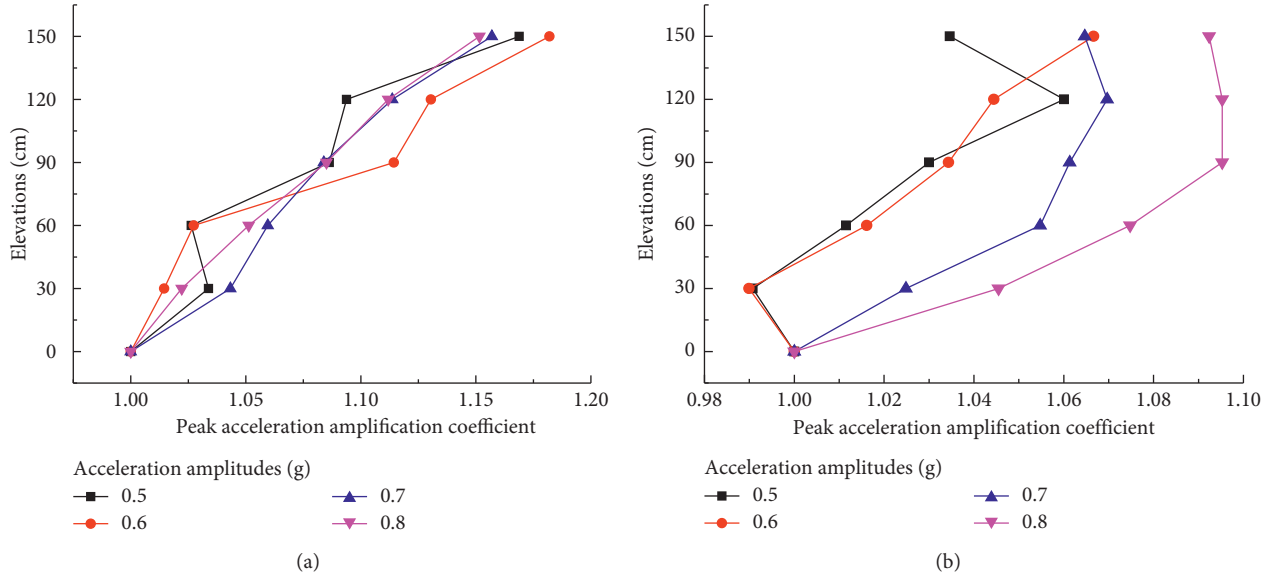

Figure 6: Changes in peak acceleration amplification coefficients of the slope surface with elevation under excitation in the X and Z bidirection. (a) Acceleration in the X-direction under excitation in the X and Z bidirection. (b) Acceleration in the Z-direction under excitation in the X and Z bidirection.

$$F_i = E \cdot \varepsilon \cdot A, \tag{1}$$

where ε, E, and A separately refer to the strain measured by the strain gauge, elastic modulus of materials, and the cross-sectional area of the corresponding model.

(2) Given axial forces F_i and F_{i+1} at two adjacent monitoring points on the anchor bolt, the average shear stress τ_i on the section of the anchor bolt between the two points can be calculated using the following formula:

$$\tau_i = \frac{F_i - F_{i+1}}{\pi \cdot d \cdot \Delta x}, \tag{2}$$

where τ_i, F_i, d, and Δx denote average shear stress on the interfaces between monitoring points i and i+1, the axial force at point i, the diameter of the corresponding model, and the distance between two points.

Formulae (1) and (2) were used for calculation. The distribution curves of axial force on the upper anchor bolt and shear stress on the anchorage interfaces were separately plotted (Figures 9 and 10). As shown in Figure 9, the peak

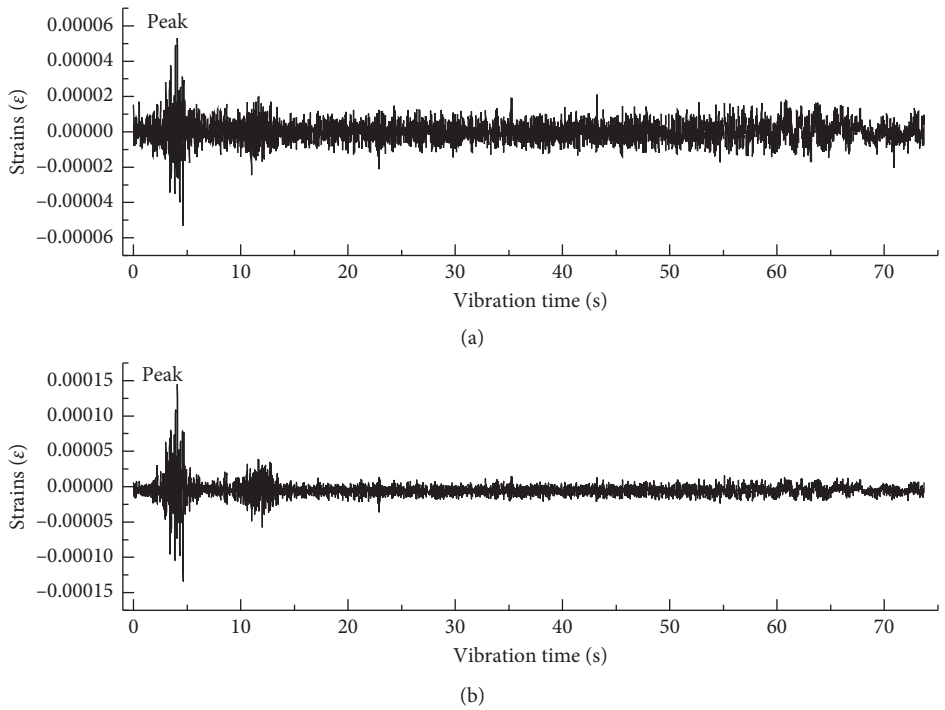

Figure 7: Time-history of strain recorded at the monitoring point of the upper anchor bolt at the weak layer. (a) Monitoring point 6 on the bolt-grout interface. (b) Monitoring point F on the grout-rock interface.

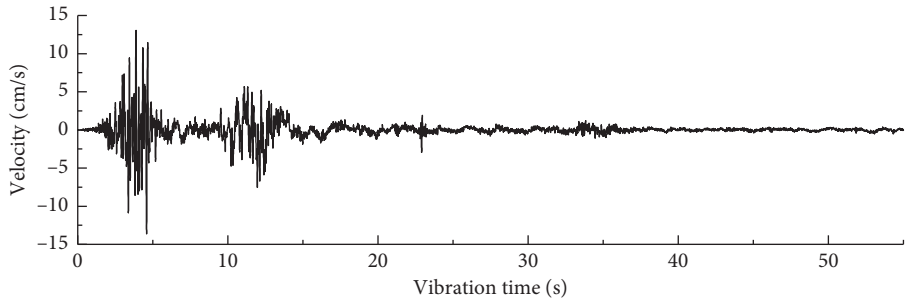

Figure 8: Time-history curve of seismic wave velocity (Wolong waves at 0.8 g).

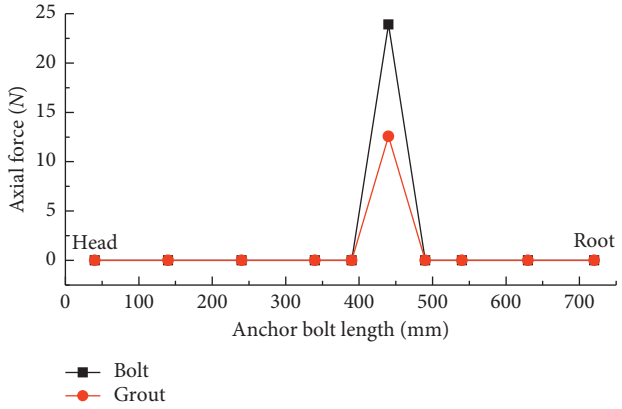

Figure 9: Distribution of axial force on the upper anchor bolt (at 4.09 s).

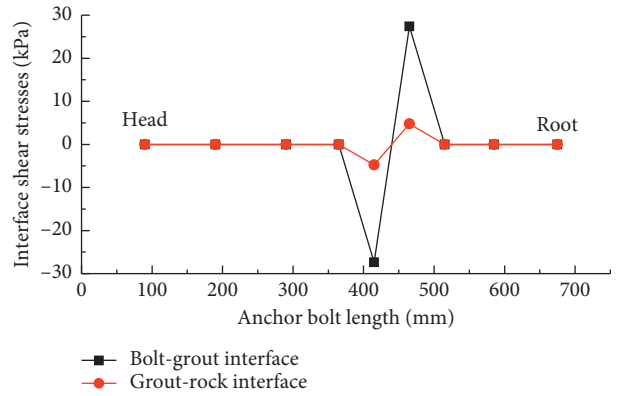

Figure 10: Distribution of shear stress on the anchorage interface of the upper anchor bolt (at 4.09 s).

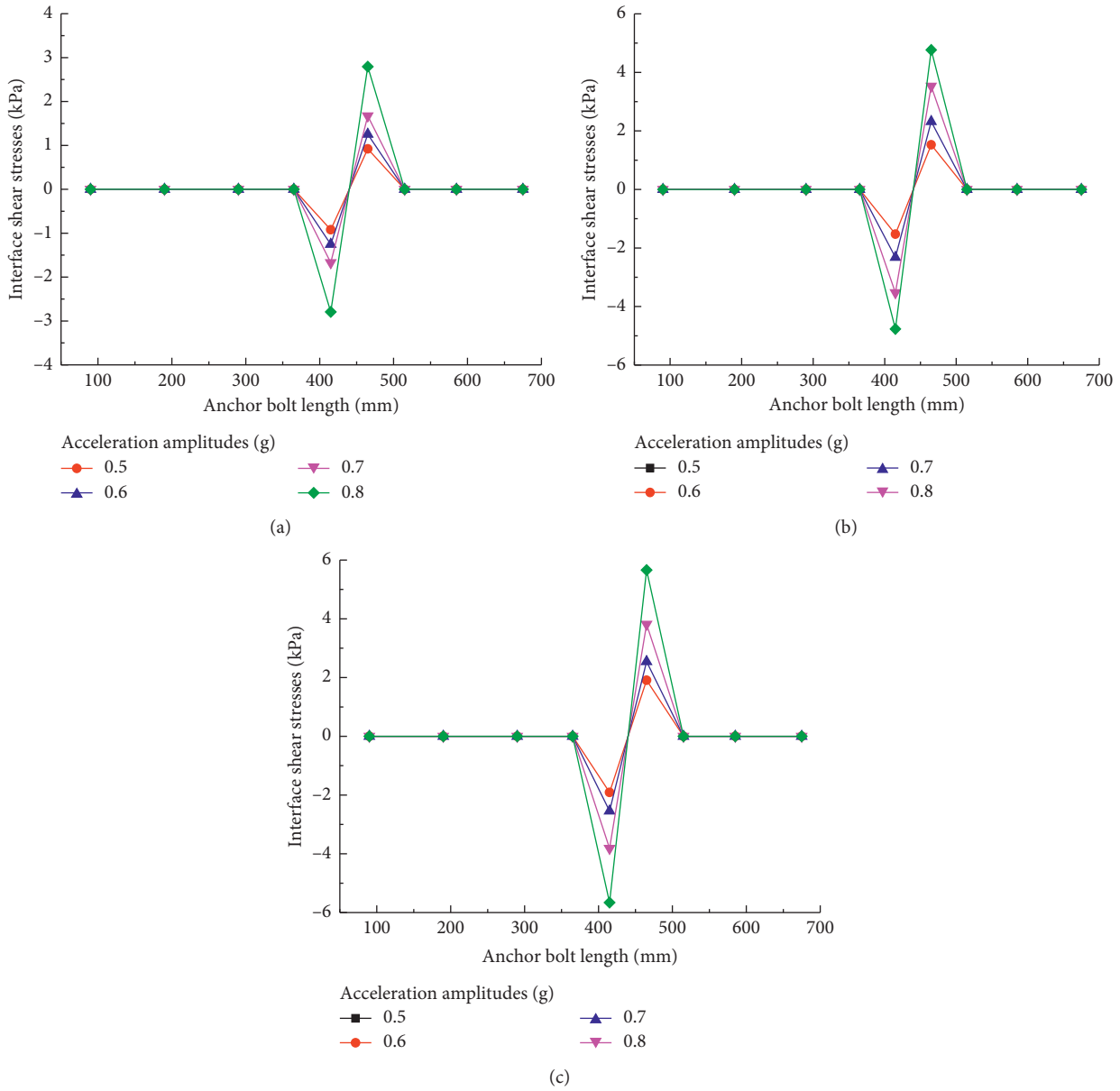

Figure 11: Distribution of shear stress on the anchorage interface under different excitation directions. (a) Excitation in the Z-unidirection. (b) Excitation in the X-unidirection. (c) Excitation in the X and Z bidirection.

axial force on the upper anchor bolt was measured at monitoring point 6 (point F) located in the weak layer, while no apparent responses were recorded by strain gauges at points 5 and 7 at each side of point 6 on the bolt-grout interface and at points E and G at each side of point F on the grout-rock interface. The axial force was large in the middle and small at two ends along the axial direction of the anchor bolt. That is to say, the axial force was largest at the weak layer and attenuated rapidly to zero towards two ends (head and root) of the anchor bolt. Figure 10 shows that the shear stress on the two anchorage interfaces of the upper anchor bolt was inversely symmetric in its distribution along the axial direction of the bolt about point 6 (point F). That is, the shear stress on the two anchorage interfaces of the section between points 5 and 6 (points E and F) in the unstable rock increased from zero to the peak negative shear stress along the axis of the anchor bolt, while that in the section from point 6 to point 7 (point F to point G) in the bedrock declined from a peak positive shear stress to zero along the axis of the bolt. The absolute values of peak positive and negative stresses were similar and the shear stress on the two anchorage interfaces was distributed in the same way; nevertheless, the peak positive and negative shear stresses on the grout-rock interface were always lower than those in corresponding section on the bolt-grout interface.

3.3. Change in Peak Shear Stress on the Anchorage Interfaces. As an apparent strain was first monitored at point F on the grout-rock interface, the shear stress on the grout-rock

interface was taken as an example for analysis. For the sake of clarity, positive values were taken for shear stresses on the interface.

The distribution of shear stress on the grout-rock interface under the action of Wolong waves with different excitation directions is shown in Figure 11. It can be seen from the figure that as the acceleration amplitude of Wolong waves in each excitation direction was increased from 0.5 g to 0.8 g, the peak shear stress on the grout-rock interface also increased. The shear stress on the interface along axial direction of the anchor bolt presented a consistent distribution under the actions of Wolong waves with different excitation directions and acceleration amplitudes: it showed an approximately inversely symmetric distribution about point F along the axis of the anchor bolt. That is, the shear stress on the grout-rock interface separately reached peak positive and negative values in sections F-G and E-F to the two sides of the weak layer along the axial direction of the anchor bolt. The peak positive and negative shear stresses had approximately equal absolute values. From these sections, the shear stress on the grout-rock interface declined to zero towards the two ends of the anchor bolt.

Figure 12 shows the change in peak shear stress on the grout-rock interface with acceleration amplitudes of Wolong waves excited in different directions. As shown in the figure, with the increase of the acceleration amplitude of Wolong waves from 0.5 g to 0.8 g, the peak shear stresses on the interface under excitation by Wolong waves in the X-unidirection were 1.53 kPa, 2.32 kPa, 3.53 kPa, and 4.77 kPa, respectively; they were 0.92 kPa, 1.26 kPa, 1.67 kPa, and 2.79 kPa under excitation by Wolong waves in the Z-unidirection; the peak shear stresses were separately 1.91 kPa, 2.54 kPa, 3.81 kPa, and 5.66 kPa on the interface when Wolong waves were excited in the X and Z bidirection. The values of peak shear stress were (in descending order) while motions were input in the X and Z bidirection, X-unidirection, and Z-unidirection. Besides, the peak shear stress on the interface under excitation by Wolong waves in the X-unidirection was similar to that when Wolong waves were input in the X and Z bidirection, while the peak shear stress was much smaller under excitation by Wolong waves in the Z-unidirection.

Figure 13 shows the change in rate of growth of peak shear stress on the grout-rock interface with the acceleration amplitude of Wolong waves. With the increase of acceleration amplitude of input motions in the X-unidirection from 0.5 g to 0.8 g, the rates of growth of the peak shear stress on the interface were 52.08%, 79.17%, and 81.25%. This indicated that the peak shear stress increased rapidly at first and then slowed down with further increases in acceleration amplitude. If Wolong waves were input in the Z-unidirection, the peak shear stress increased by 35.90%, 45.30%, and 121.75% successively with the acceleration amplitude of input motions, which suggested that the peak shear stress increased slightly and then significantly with increasing acceleration amplitude. The rates of growth of the peak shear stress on the interface were 33.33%, 66.67%, and 96.67% when the Wolong waves were input in the X and Z bidirection. The peak shear stress increased in a quasilinear manner with the acceleration amplitude of the input motions.

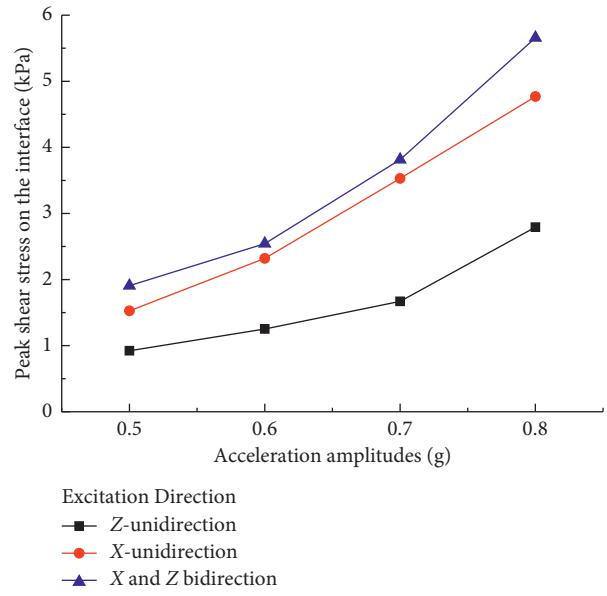

Figure 12: Change in peak shear stress on the interface with acceleration amplitudes of Wolong waves.

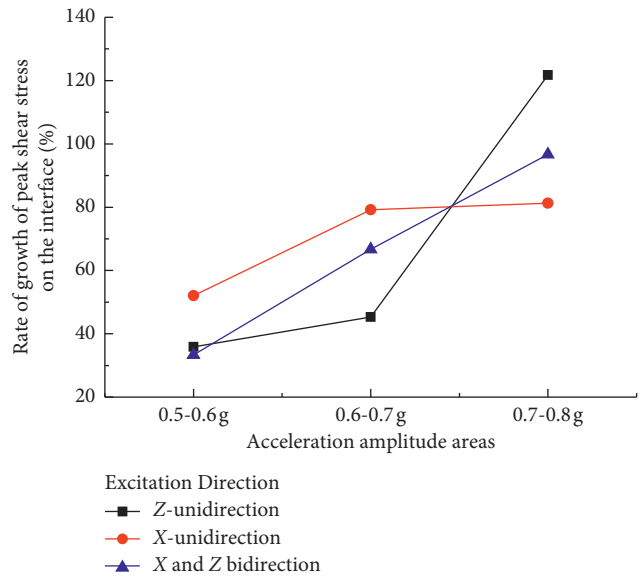

Figure 13: Change in rate of growth of peak shear stress on the interface with acceleration amplitudes of Wolong waves.

Collectively, the peak shear stress on the interface when seismic waves were input in the X-unidirection was similar to that under excitation by seismic waves in the X and Z bidirection. The result implied that the X-direction seismic waves in the seismic waves input in the X and Z bidirection played a dominant role in the shear effects on the anchorage interfaces. The change in the rate of growth of peak shear stress on the interface with the acceleration amplitude of seismic waves indicated that the effects of Z-direction seismic waves therein upon the shear effects on the

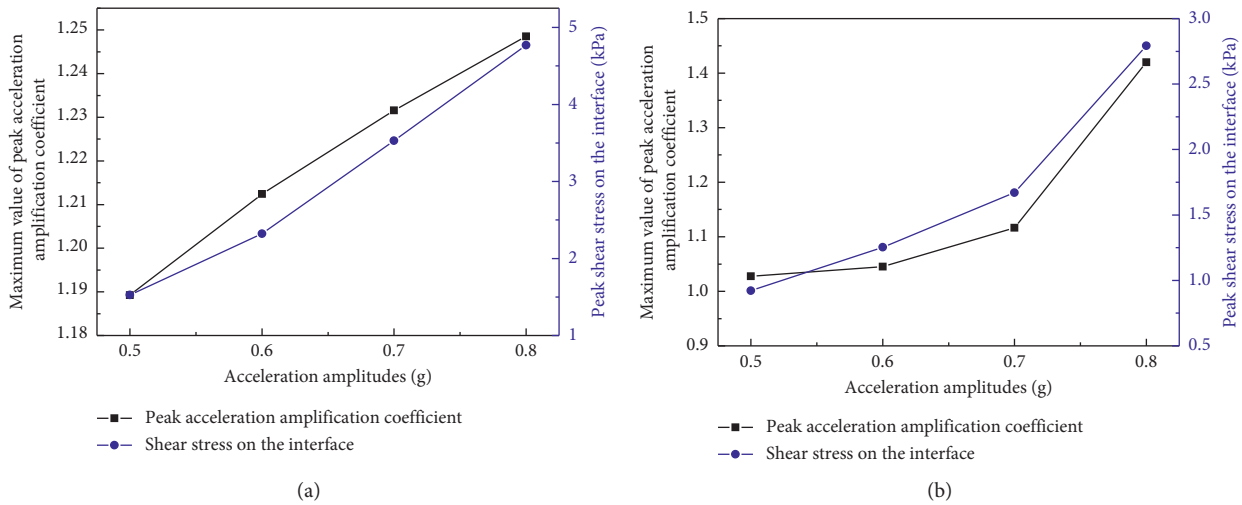

Figure 14: Comparison of changes in shear stress on anchorage interfaces and acceleration response. (a) Excitation in the X-unidirection. (b) Excitation in the Z-unidirection.

anchorage interfaces were also nonnegligible. This matches the vertical seismic responses measured in the Wenchuan earthquake [20].

3.4. Relationship between Shear Effects on the Anchorage Interfaces and the Acceleration Response. By combining the shear effects on the anchorage interfaces and the acceleration seismic response of the slope, they were found to have a close relationship. Firstly, the maximum value of peak acceleration amplification coefficient in the X-direction on the slope surface was recorded at the slope shoulder and that in the Z-direction was also found in the vicinity of the slope shoulder. The upper part (90 to 150 cm) of the slope surface showed an apparent acceleration amplification effect, so the upper anchor bolt closest to the slope shoulder among the three monitored anchor bolts was the first to show shear effects on anchorage interfaces. Under this condition, there were insignificant acceleration amplification effects in the middle and lower parts (0 to 90 cm) of the slope surface, so no shear effects were observed on the anchorage interfaces of middle and lower anchor bolts in the area.

Secondly, the maximum value of peak acceleration amplification coefficient of the slope surface was closely related to the peak shear stress on the interfaces. As the synthesised motions input in the X and Z bidirection comprise two motions input in the X-unidirection and Z-unidirection, the resulting peak acceleration amplification coefficients of the slope surface are a result of the interplay of motions input in the X-unidirection and Z-unidirection, which is not a typical case used for comparison. Therefore, only the change in maximum value of peak acceleration amplification coefficient and peak shear stress on the interfaces separately under actions of motions input in the X-unidirection and Z-unidirection with the acceleration amplitude of Wolong waves was compared. As shown in Figure 14(a), under the action of Wolong waves in the X-unidirection with an amplitude of 0.5 g to 0.8 g, both the maximum value of peak acceleration amplification coefficient in the X-direction of the slope surface and the peak shear stress on the interfaces increased in a quasilinear manner with the acceleration amplitude of the Wolong waves. It can be seen from Figure 14(b) that the maximum value of peak acceleration amplification coefficient in the Z-direction of the slope surface and the peak shear stress on the interfaces grew slowly when Wolong waves with an amplitude of 0.5 g to 0.7 g were input in the Z-unidirection; as the acceleration amplitude of the input motions was increased from 0.7 g to 0.8 g, both increased rapidly, that is, they both increased slowly at first and then rapidly with the increased acceleration amplitude of the input motions.

By comparing the trends in maximum value of peak acceleration amplification coefficient of the slope surface and the peak shear stress on the anchorage interfaces with the acceleration amplitude of input seismic waves, it can be found that they showed similar trends. This indicated that with the increased acceleration amplitude of seismic waves, the slope exhibited a stronger seismic response and increased deformation. Under this condition, the anchor system played its anchoring effect to restrain deformation, and therefore the shear effects on the anchorage interfaces became more significant.

4. Conclusion

A large-scale shaking table model test was performed to explore the shear effects on two anchorage interfaces and seismic responses of the rock slope under seismic action for the first time, which is important to understanding the anchoring of rock and soil masses. The main conclusions are drawn as follows:

(1) Under seismic action, it was the top of the slope that was subjected to tensile deformation first. The shear effects were first recorded at the grout-rock interface of the upper anchor bolt at the weak layer, and shear stress was distributed in a similar manner on the two anchorage interfaces: the peak positive and negative shear stresses were distributed on each side of the

weak layer and had similar absolute values, which reduced to zero towards the two ends of the anchor bolt.

(2) Under seismic action in different excitation directions, the distribution of shear stress was unchanged on the anchorage interfaces along the axis of the anchor bolt. The peak shear stresses were listed (in descending order) when inputting seismic waves in the X and Z bidirection, X-unidirection, and Z-unidirection, and they increased with the increasing intensity of ground motion, while peak shear stress grew at different rates under seismic action in different excitation directions.

(3) X-direction seismic waves in the seismic waves excited in the X and Z bidirection played the leading role in the shear effects on the anchorage interfaces, while Z-direction seismic waves therein were also nonnegligible.

(4) The peak acceleration amplification coefficients in the X and Z directions of the slope surface under seismic actions both increased with the increased intensity of ground motion and with elevation of the slope surface. Moreover, the upper part of the slope surface presented the most prominent elevation amplification effect.

(5) The shear effects on the anchorage interfaces were closely related to the seismic response of the slope surface: as the seismic response increased, the shear effects on the anchorage interfaces were also intensified.

Data Availability

The data used to support the findings of this study are available from the corresponding author upon request.

Conflicts of Interest

The authors declare that they have no conflicts of interest.

Acknowledgments

The authors are grateful for the assistance rendered by Master's candidates Yao Guo-qiang and Xiao Peng under the supervision of Professor Yan Zhixin for their work in the experiment. This study was supported by a general programme of the National Natural Science Foundation of China (grant nos. 41372307 and 51779021).

References

[1] F. F. Ren, Z. J. Yang, and J. F. Chen, "An analytical analysis of the full-range behavior of grouted rockbolts based on a tri-linear bond-slip model," *Construction and Building Materials*, vol. 24, no. 2, pp. 361–370, 2010.

[2] L. Blanco Martín, M. Tijani, F. Hadj-Hassen, and A. Noiret, "Assessment of the bolt-grout interface behaviour of fully grouted rockbolts from laboratory experiments under axial loads," *International Journal of Rock Mechanics and Mining Sciences*, vol. 63, pp. 50–61, 2013.

[3] S. Ma, J. Nemcik, and N. Aziz, "An analytical model of fully grouted rock bolts subjected to tensile load," *Construction and Building Materials*, vol. 49, pp. 519–526, 2013.

[4] C.-A You, "Mechanical analysis of the fully bonded anchor," *Rock Mechanics and Engineering*, vol. 19, no. 3, pp. 339–341, 2000.

[5] Yi-P Luo, S. Shi, and Y. A. N. Zhi-xin, "Shear interaction of anchorage body and rock and soil interface under the action of uplift load," *Journal of China Coal Society*, vol. 40, no. 1, pp. 58–64, 2015.

[6] F.-F Ren, C. Xu, and C. Wen-wu, "Numerical simulation on load transfer mechanism of multi-interface composite rock-bolt," *Journal of Tongji University (natural Science)*, vol. 39, no. 12, pp. 1753–1759, 2011.

[7] D. Shen, Y. Ji, F.-F Yin, and J. Zhang, "Dynamic bond stress-slip relationship between basalt FRP sheet and concrete under initial static loading," *Journal of Composites for Construction*, vol. 19, no. 6, Article ID 04015012, 2015.

[8] A. Mortazavi and F. Tabatabaei Alavi, "A numerical study of the behavior of fully grouted rockbolts under dynamic loading," *Soil Dynamics and Earthquake Engineering*, vol. 54, pp. 66–72, 2013.

[9] Yi-P Tan and Z.-Q Zeng, "Pull-out tests on anchor bolts under simple harmonic waves," *Chinese Journal of Geotechnical Engineering*, vol. 35, no. 3, pp. 409–414, 2013.

[10] Z.-X. Yan, J. Duan, P. Jiang, Z.-Z. Liu, H.-L. Zhao, and W.-G. Huang, "Finite difference method for dynamic response analysis of anchorage system," *Journal of Central South University*, vol. 21, no. 3, pp. 1098–1106, 2014.

[11] J. Duan, Z.-X. Yan, R.-J. Guo, and Z.-H. Ren, "Response analysis of frame supporting structure of slope under harmonic vibration," *Mathematical Problems in Engineering*, vol. 2014, Article ID 603863, 13 pages, 2014.

[12] Y.-S. Hong, R.-H. Chen, C.-S. Wu, and J.-R. Chen, "Shaking table tests and stability analysis of steep nailed slopes," *Canadian Geotechnical Journal*, vol. 42, no. 5, pp. 1264–1279, 2005.

[13] H. Jian-Bin, L. I. Jin-he, T. Cheng et al., "Experimental study of slopes supported with framed anchors on shaking table," *Chinese Journal of Rock Mechanics and Engineering*, vol. 34, no. 2, pp. 293–304, 2015, in Chinese.

[14] H. Qiu-Xiang, Xu Xiang-tao, C. Xu et al., "Dynamic response characteristics of an anchored rock slope during Wenchuan earthquake," *Rock and Soil Mechanics*, vol. 37, no. 6, pp. 1729–1736, 2016, in Chinese.

[15] Y. Zhi-Xin, L.-P. Zhang, P. Jiang et al., "Dynamic response of anchoring overlying red clay rock slope under earthquake action," *Rock and Soil Mechanics*, vol. 35, no. 3, pp. 753–758, 2014.

[16] Y. Zhi-Xin, Z. Long, X.-L. Zhou et al., "Numeral analysis of anchoring parameters for bolt in rock slope anchored interface shear action under earthquake," *Journal of China Coal Society*, vol. 42, no. 10, pp. 2537–2544, 2017.

[17] Y. Zhi-Xin, Z. Long, Q Wen-Rui et al., "Analysis of shear action on anchorage interface of rock slope with weak layer under earthquake," *Rock and Soil Mechanics*, vol. 40, no. 7, pp. 1–9, 2019.

[18] X.-C Yao, L. I. Ning, and C. Yun-Sheng, "Theoretical solution for shear stresses on interface of fully grouted bolt in tunnels," *Chinese Journal of Rock Mechanics and Engineering*, vol. 24, no. 17, pp. 2272–2276, 2005.

[19] Gb 50011-2001, *Code for Seismic Design of buildings[S]*, China Architecture and Building Press, Beijing, China, 2001.

[20] J.-J. Xie, Z.-P. Wen, M.-T. Gao et al., "Characteristics of near-fault vertical and horizontal ground motion from the 2008 Wenchuan earthquake," *Chinese Journal of Geophysics*, vol. 53, no. 8, pp. 1796–1805, 2010, in Chinese.